Surfaces and Interfaces 66 (2025) 106560

Contents lists available at ScienceDirect

Surfaces and Interfaces

journal homepage: www.sciencedirect.com/journal/surfaces-and-interfaces

Study on CO_2 gasification mechanism of bituminous coal coke by *in-situ* measurement and DFT calculation

Hui Luo [a,b], Yaqiong Wang [b], Weiwei Xuan [b,c], Jiansheng Zhang [a,b,*]

[a] Department of Energy and Power Engineering, Tsinghua University, Beijing 100084, China
[b] Shanxi Research Institute of Huairou Laboratory, Taiyuan 030000, China
[c] School of Energy and Environmental Engineering, University of Science and Technology Beijing, Beijing 100083, China

ARTICLE INFO

Keywords:
CO_2 gasification
Coal coke
Carbon-oxygen complexes
In-situ characterization
DFT calculations

ABSTRACT

CO_2 gasification with coal/coke is an important technology that can convert and store CO_2 into chemical products in a massive and feasible way. Understanding the mechanism of the CO_2-coke gasification is the basis for the industrialization and designation of CO_2 gasifier, which provide fundamental technology for Carbon Capture, Utilization and Storage (CCUS). In this work, the CO_2 gasification process was studied by Thermogravimetric-Fourier Transform Infrared Spectrometer Mass Spectrometer (TG-FTIR), Thermogravimetric-Mass Spectrometer (TG-MS) and *in-situ* Raman. The atomic level mechanism of CO_2 reaction with coke was analyzed by Density Functional Theory (DFT) calculation. The result shows that the COO-group in the coke is the CO precursor from the CO_2-coke gasification. In the process of pre-adsorption of CO_2 on the surface of coal coke, the C—O-O- group is formed, and the degree of the electron conjugation of the aromatic ring pi is decreased, and the strength of intermolecular mayer bond is decreased, destroying the aromaticity of the coal coke molecular surface, exposing more active sites, accelerating the gasification reaction of coal coke, and promoting CO desorption. And the entire gasification process is the endothermic reaction with 1.60 eV.

1. Introduction

CO_2 gasification with coal/coke is an important technology that can convert and store CO_2 into chemical products in a massive and feasible way. And it provides fundamental technology for Carbon Capture, Utilization and Storage (CCUS). By gasification of CO_2 and coal/coke into coal gas, on the one hand, the emission of pollutants can be greatly reduced, on the other hand, the utilization efficiency of coal/coke can be improved [1–3].

Understanding the mechanism of the CO_2-coke gasification is the basis for the industrialization and designation of CO_2 gasifier. Current work is limited to the optimization of reaction conditions and gasification products during gasification, there are fewer studies on the mechanism of the CO_2-coke gasification reaction process [4–9]. Zhang et al. [10] compared the effect of CO_2 concentration (100 %CO_2, 50 %CO_2/50 %H_2O, 95 %H_2O/5 %CO_2) on the gasification characteristics and conversion rate of Xiaolongtan coal coke by thermogravimetric analyzer (TG). The result showed that average reaction rate of coal coke with H_2O is about three times that of CO_2. This result was consistent with the findings of Lan et al. [11]. Roberts et al. [12] pointed out that H_2O and CO_2 compete at the common active site and CO_2 has an inhibitory effect on the C—H_2O reaction. However, it has been pointed out that H_2O and CO_2 have some synergistic effects, and their interaction improves the physical structure of coal and accelerates the rate of the co-gasification reaction [13,14]. As noted above, traditional characterization analyses focus on characterizing coal coke structures and syngas products components. However, the results may vary on the analytical environment. *In-situ* process analysis techniques enable the characterization of elemental migration, functional group evolution, aromatic structure development and other processes during coal coke gasification reactions under real conditions. These technical characterizations were widely used in coal and biomass pyrolysis, but less in coal coke gasification [15]. Song et al. [16] used Gas Chromatography-Mass Spectrometry (GC–MS) coupled with a Gas Chromatograph (GC) and a Mass Spectrometer (MS) to characterize the composition of gases and tars by coal pyrolysis, and the results showed that intrinsic minerals also promoted the cracking of aliphatic hydrocarbons, polycyclic aromatic hydrocarbons (PAHs), and oxygenates in the pyrolysis tars. The GC–MS could be applied to quantitative analysis of gaseous products in thermal conversion processes [17–20]. As an *in-situ* characterization and analysis

* Corresponding author at: Department of Energy and Power Engineering, Tsinghua University, Beijing 100084, China.
E-mail address: zhang-jsh@tsinghua.edu.cn (J. Zhang).

https://doi.org/10.1016/j.surfin.2025.106560
Received 7 February 2025; Received in revised form 11 April 2025; Accepted 24 April 2025
Available online 25 April 2025

Table 1
The proximate and ultimate analysis of the bituminous coal and coal coke.

Sample	Proximate analysis (wt.%)				ultimate analysis (wt.%)			
	M_{ad}	A_{ad}	V_{ad}	FC_{ad}	C_{ad}	H_{ad}	N_{ad}	S_{ad}
Bituminous coal	0.91	9.40	33.19	56.50	73.44	4.49	1.01	0.82
Coal coke	0.95	12.08	2.60	84.37	85.61	1.34	1.19	0.85

Note: "ad" denotes the air-dried basis.

technique, the TG-FTIR-GC–MS, which could thoroughly combine the techniques of TG, Fourier Transform Infrared Spectrometer (FTIR), GC, MS, could be used to real-time detect sample loss of weight, functional groups and volatile components in the thermal reforming process [21]. Researchers have carried out a lot of studies on the thermal conversion process of coal by this technique. Lei et al. [22] investigated the pyrolysis mechanism of Shenfu bituminous coal by TG-FTIR-GC–MS. Su et al. [23] used TG-FTIR-GC–MS to investigate the co-pyrolysis characteristics of Huangling low-rank coal (SJC) and coking coal (JM) and their interactions. The results showed that JM promoted the pyrolysis of SJC by increasing the number of colloids and providing the conditions for the interaction reaction between pyrolysis products. With SJC and JM as the hydrogen donor, the [H] and free radicals generated during pyrolysis favored the hydrogenation reaction and greatly reduced the light fraction in the tar. The *in-situ* Raman technique has also been received attention from researchers in the field of carbon-based materials thermal conversion. Zhu et al. [24] used *in-situ* Raman and a fixed-bed reactor to characterize the evolution of the coke structure and the formation behavior of the product gases. The results showed that the FWHM of the D_1 and G bands and the band area ratios of I_{D1}/I_G, I_{D3}/I_G, and I_{D4}/I_G increased with increasing temperature. Whereas the peak of D_1 and G bands and the ratio of I_G/I_{All} decreased, indicating a decrease in the ordering of the carbon structure. Therefore, it is necessary to investigate the changes in surface functional groups and structure during coal coke gasification, with the help of advanced on-line and *in-situ* analysis techniques. In recent years, the combination of Density Functional Theory (DFT) calculations and experiments has been allowed the transformation of macroscopic reaction phenomena into microscopic molecular collisions, which leads new directions for in-depth study on mechanisms [25–27]. Xu et al. [28] used a six-membered ring to simulate the gasification reaction mechanism of coke under H_2O and CO_2 atmospheres. The results showed that H_2O reacted with carbon more easily than CO_2 due to the lower energy barrier for adsorption and generation of H_2 by H_2O molecules. Dong et al. [29] explored the change of functional groups of coal after microwave treatment and probed the reaction paths of two $C_{10}H_{10}O_4$ isomers under CO_2. Zhao et al. [30] constructed a 6-ring sawtooth-type model to further investigate the steam gasification reaction paths. The results showed that the aromaticity of the graphite model edges was linearly related to the desorption of CO. H atoms in H_2O were transferred to the edges of the graphite model, destroying the aromaticity of the edge carbon structure, which was favorable for the subsequent desorption process. And it might be the reason for the higher reactivity of steam compared with CO_2 gasification. However, the credibility of DFT calculations for the CO_2-coke gasification in the existing work also needs to be improved due to the complex structure of the coal coke molecules. In conclusion, the current studies on the influence mechanism of the CO_2-coke gasification process lack systematic in-depth investigation. Therefore, it is necessary to analyze the volatile products of coal coke under gasification conditions with the help of advanced on-line and *in situ* testing methods to explore the coal coke gasification process, carry out the simulation of the CO_2-coke process by DFT calculations, and combine the results of characterization analyses to improve the credibility of the calculation results and explore the mechanism of the CO_2 gasification reaction of coal coke.

In summary, the typical Shenmu bituminous coal from Yulin was chosen as the coal coke raw material. The CO_2 gasification process was studied by TG-FTIR, TG-MS, *in-situ* Raman to characterized the CO_2-coke gasification varying with reactants and temperature. In addition, the simulation of the CO_2-coke gasification process was also calculated by DFT method, to reveal the mechanism of CO_2 gasification. Furthermore, the findings hope to provide data support and theoretical basis for the design of gasifier.

2. Materials and methods

2.1. Sample preparation

The coal coke used in this work was prepared form Yulin Shenmu bituminous coal, and the results of proximate and ultimate analysis of bituminous coal and coal coke are shown in Table 1. It can be found that the volatiles and fixed carbon contents of bituminous coal are high, which are 33.19 wt.% and 56.60 wt.%, respectively. After the preparation of coal coke, the volatiles content of the sample was significantly reduced to 2.60 wt.%, and the ash content of coal coke is 12.08 wt.%.

The preparation process of coal coke is briefly described as follows:

The appropriate amount of the bituminous coal was taken the high-temperature tube furnace. 200 mL/min of N_2 was introduced in the high-temperature tube furnace with heating rate of 10 °C/min to 800 °C, and then stayed at 800 °C for 30 min. Lastly, the sample was cooled in N_2 to obtain coal coke. The coal coke production rate was 59.80 % ~ 68.20 %. Finally, the 75~105 μm coal coke was obtained by the standard sieve.

2.2. Coal coke gasification characteristics test

The thermogravimetric analyzer (TG, Netzsch STA 449F5, Germany) was used to explore the CO_2-coke gasification characteristics. The test procedure was as follows: 15 ± 0.3 mg of coal coke was taken in a crucible and placed on the thermogravimetric analyzer, and the temperature of the furnace chamber was increased from room temperature to 800 °C at a total flow rate of 100 ml/min under N_2 atmosphere by 10 °C/min, and then the experimental atmosphere was changed to N_2 + (20 %, 40 %, 60 %, 80 %) CO_2, and then increased to 1200 °C by 10 °C/min.

2.3. Characterization of sample

To discuss the relationship between the structure and the gasification characteristics of coal coke, some characterization methods were used in this work. X-ray photoelectron spectroscopy (XPS, Thermo scientific Co., USA) was chosen to analyze the distribution of oxygen-containing functional groups on the surface of the coal coke. IS50 Fourier Transform Infrared Spectrometer (FTIR, Thermo Scientific Co., USA) was used to analyze the surface functional groups of the coal coke. The carbon crystal structure was measured by Raman spectrometer (Raman, Thermo Fisher Scientific DXR2xi, USA). The gasification characteristics and volatile gases of the coal coke were measured by the thermogravimetric analyzer (TG, NETZSCH STA 449 F3, Germany) and the FTIR spectrometer (Bruker Tensor II, Germany), which were connected by a PTFE transmission line at 150 °C to avoid condensation of volatile products during gasification. The *in-situ* Raman spectroscopy system (Thermo Fisher DXR2xi, USA) was used to measure the evolution of coal coke. In addition, the thermogravimetric analyzer (TG, NETZSCH STA 449 F3, Germany) and the Mass Spectrometer (Master MS, Bruker, USA)

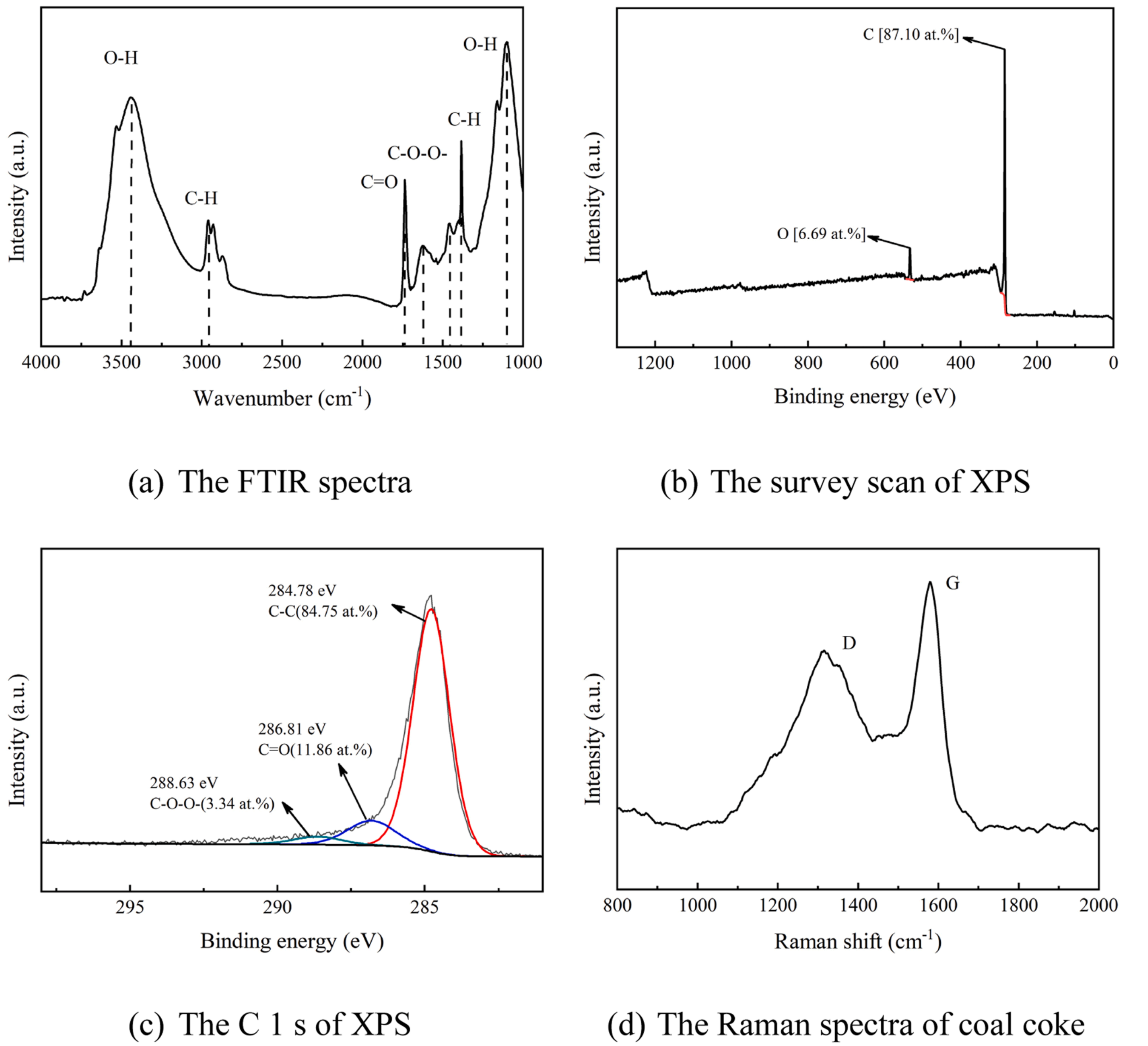

Fig. 1. FTIR spectra, XPS spectra and Raman spectra of coal coke. (a) FTIR spectra; (b) survey scan of XPS; (c) C 1 s of XPS; (d) Raman spectra.

were used to qualitatively analyze the coal coke gasification products.

2.4. Calculation method

All density-functional (DFT) calculations in this work were carried out by Gaussian 16, with geometrical optimization and frequency calculations for all the substances in the reaction in the B3lyp/6–31 (d, p) basis set, and zero-point energy calculations for the optimized structures in the B3lyp/deftzvp basis set. The wave functions output from Gaussian 16 were analyzed by Multiwfn and VMD software [31]. The activation energy (Δ_E) was calculated from the free energy difference before and after the reactants.

$$\Delta E = E_a + E_b - E_{ab} \tag{1}$$

Where, E_a denotes the energy before reaction of reactant a, kJ/mol; E_b denotes the energy before reaction of reactant b, kJ/mol; and E_{ad} denotes the energy of the system after reaction, kJ/mol. When the value of Δ_E is positive, it means that the reaction is an adsorptive reaction, and vice versa is an exothermic reaction.

3. Results and discussion

3.1. Characterisation of coal coke structure

The distribution pattern of functional groups on the coal coke surface is shown in Fig. 1(a), and the infrared spectrum near 3436 cm^{-1} and 1000 cm^{-1} are attributed to O—H stretching vibration. It indicates the presence of adsorbed chemical water molecules and O—H groups on the coal coke surface. 2956 cm^{-1} and 1384 cm^{-1} are the aromatic C—H vibration, and 1457 cm^{-1} and 1625~1735 cm^{-1} belong to the COO- vibration and $C = O$ stretching vibration, respectively [32]. The XPS spectra of the C 1 s orbitals on the surface of the coal coke are shown in Fig. 1(b), (c), which shows that the coal coke surface is rich in elemental C with the relative content of 87.10 at.%, and the O content is only 6.69 at.%, which suggests that the coal coke has a good gasification potential. Peaking the C 1 s orbitals on the surface of the coal coke, the result is shown in Fig. 1(c). The relative content of C—C (284.78 eV) is as high as 84.75 at.%, which suggests that the coal coke mainly constructs the macromolecular skeleton with benzene rings. In addition, the

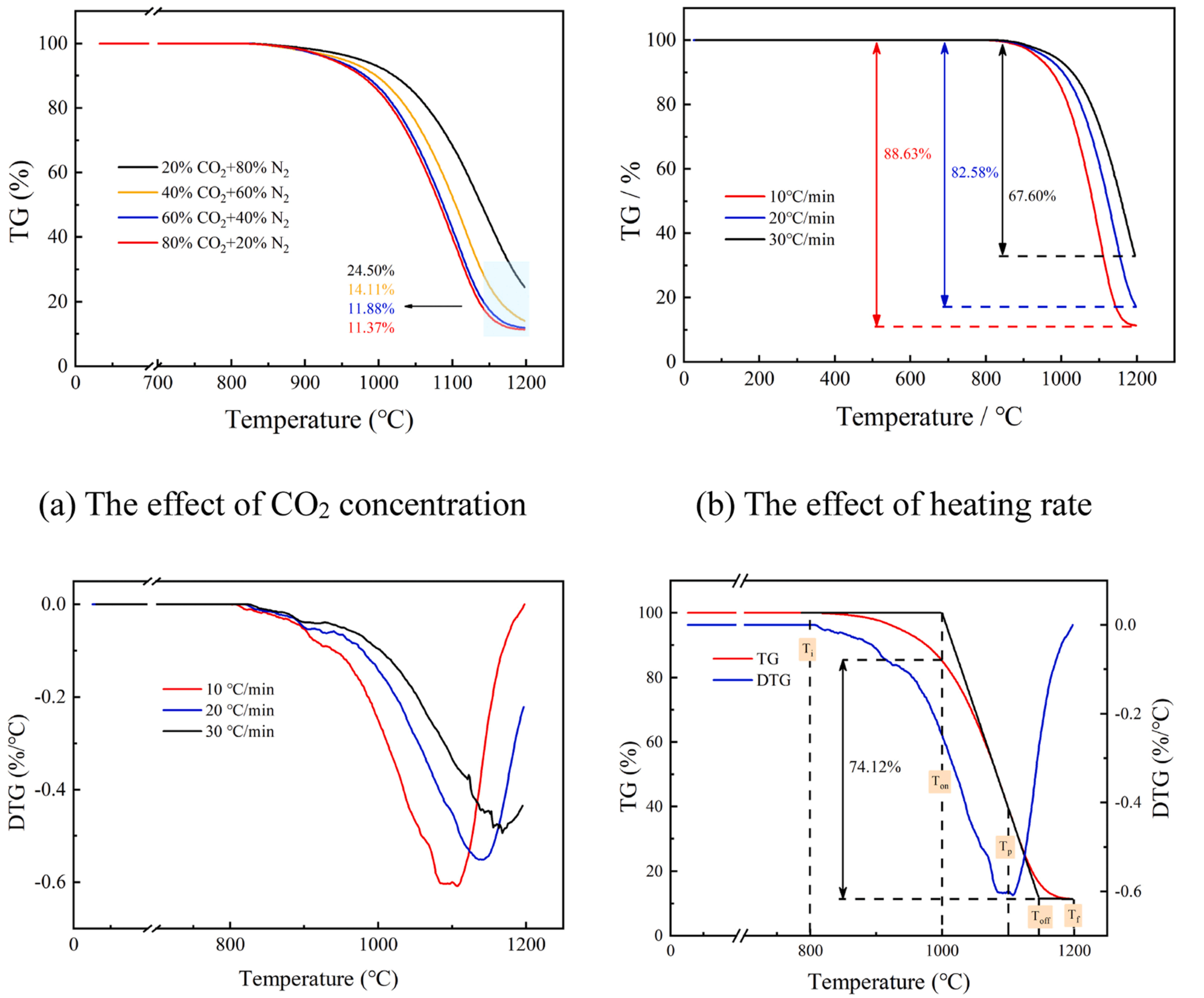

(a) The effect of CO_2 concentration

(b) The effect of heating rate

(c) The DTG curves of coal coke in different heating rate

(d) The TG and DTG curves of coal coke in 80%CO_2+20%N_2

Fig. 2. The TG/DTG results of coal coke.

carbon-oxygen functional groups on the surface of coal coke are mainly $C = O$ (286.81 eV) and C—O-O- (288.63 eV). Some works show that CO_2 is more easily attached to the C atoms near functional group and subsequently undergoes a desorption reaction [33]. This result is corroborated with the FTIR analysis. Raman spectral analysis result of the coal coke surface is shown in Fig. 1(d), and two characteristic peaks 1580 cm^{-1} (G band) and 1350 cm^{-1} (D band) exist on the coal coke surface, where the G band is attributed to the vibrational mode of an ideal graphite lattice with symmetry, and the D band denotes the residual charcoal sites with disordered structure [34]. The wave peaks in the G band are higher compared to the D band, which indicates that the coal coke molecules are mainly dominated by the benzene ring structure. Meanwhile, the half-peak width of the D band is larger, which indicates that functional groups still exist at the edges of the coal coke molecule. Combining the results of FTIR, XPS and Raman analyses, it can be found that the coal coke molecules are mainly ordered carbons dominated by C—C structures, and the disordered carbon structures (e.g., aliphatic, C—O-O- and $C = O$, etc.). It provides a reference for modelling the coal coke molecule during DFT calculations.

3.2. TG analysis

The effect of CO_2 concentration on the gasification characteristics of coal coke is shown in Fig. 2(a). The gasification occurs at 800 ~1200 °C, after reaching the gasification temperature (800 °C) and switching to the mixed gasification atmosphere doped with CO_2, the weight loss rate of coal coke is increasing with the increase of CO_2 concentration. The final weight loss of coal coke is 75.50 % under 20 %CO_2 atmosphere, while the final weight loss reaches 88.63 % under 80 %CO_2 atmosphere. It can be found that CO_2 promotes the gasification process of coal coke, which may be due to the reaction of CO_2 with C on the surface of coal coke to produce more CO, this result is consistent with Cai et al. [35]. Based on the 80 %CO_2 atmosphere, this paper continues to investigate the effect of the heating rate on the gasification characteristics of coal coke, and the results are shown in Fig. 2(b), (c), which shows that the final weight loss of coal coke decreases with the acceleration of the heating rate. At

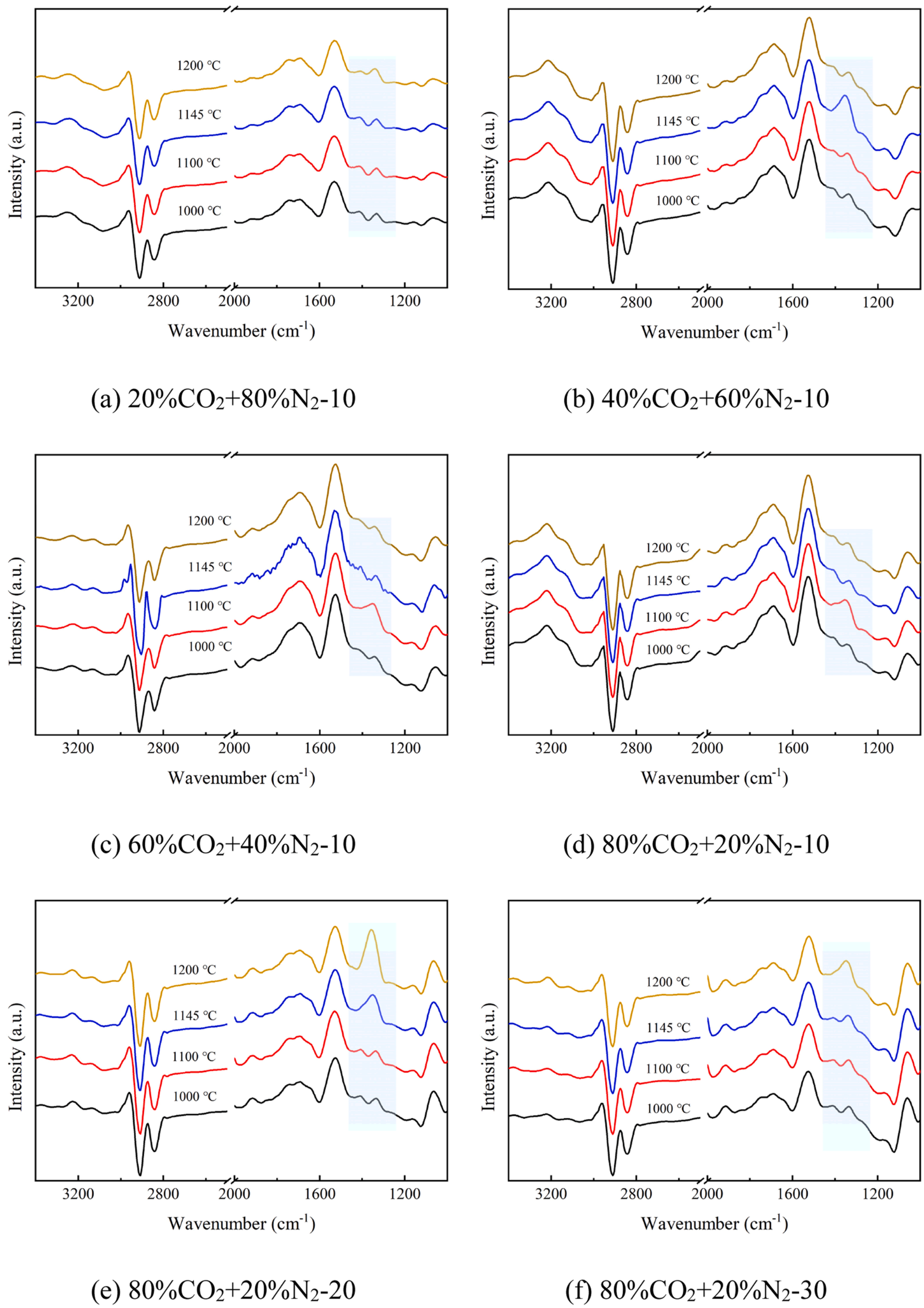

Fig. 3. TG-FTIR spectra of coal coke.

Table 2
Typical absorption peaks and their corresponding volatile gas species.

Wavenumber (cm^{-1})	Functional group	Possible species
3200–2877	C-H vibration	CH_4
1751–1689	$C=O$ vibration	Ketones, acids, esters, etc.
1531–1523	C—C vibration	Aromatic
1338–1407	C-O-O- vibration	Ester, acid
1204–1122	C—O vibration O-H vibration	Aniline
1157–1052	O—H vibration C-O(H) vibration	Alcohols, phenols

30 °C/min, the final weight loss of coal coke was only 67.60 %. The peak temperature of the DTG curve is shifted toward higher temperatures with increasing heating rate. Rapid heating leads to an increased temperature gradient between the inside and outside of the coal coke particles, where the internal temperature is lower than the external one, and a higher apparent temperature is required to trigger the reaction [36]. The apparent activation energy of the reaction also increases when the heating rate increases, requiring high temperature compensation [37]. Wang et al. [38] had similar results when investigating the gasification characteristics of corn stover. The higher gasification rate (30 °C/min) made the gasification process of coal coke incomplete, while the lower gasification rate (10 °C/min) contributes to the timely emission of CO and promoted the pore structure of the coal coke.

The TG and DTG curves of coal coke in 80 %CO_2+20 %N_2 are shown in Fig. 2(d), and T_i/T_f, T_{on}/T_{off}, and T_p represent the gasification start/end temperature, the main gasification reaction start/end temperature, and the maximum weight loss fitting temperature, respectively. The main gasification reaction of coal coke in 80 %CO_2+20 %N_2 occurs at 1000–1145 °C. At 1000 °C, the weight loss of coal coke is only 14.93 %, while at 1145 °C, the weight loss of coal coke reaches 81.93 %. In this temperature band, the weight loss rate of coal coke reaches 74.12 %, in which the fastest reaction rate occurs at 1100 °C with a weight loss ratio of 60.56 %.

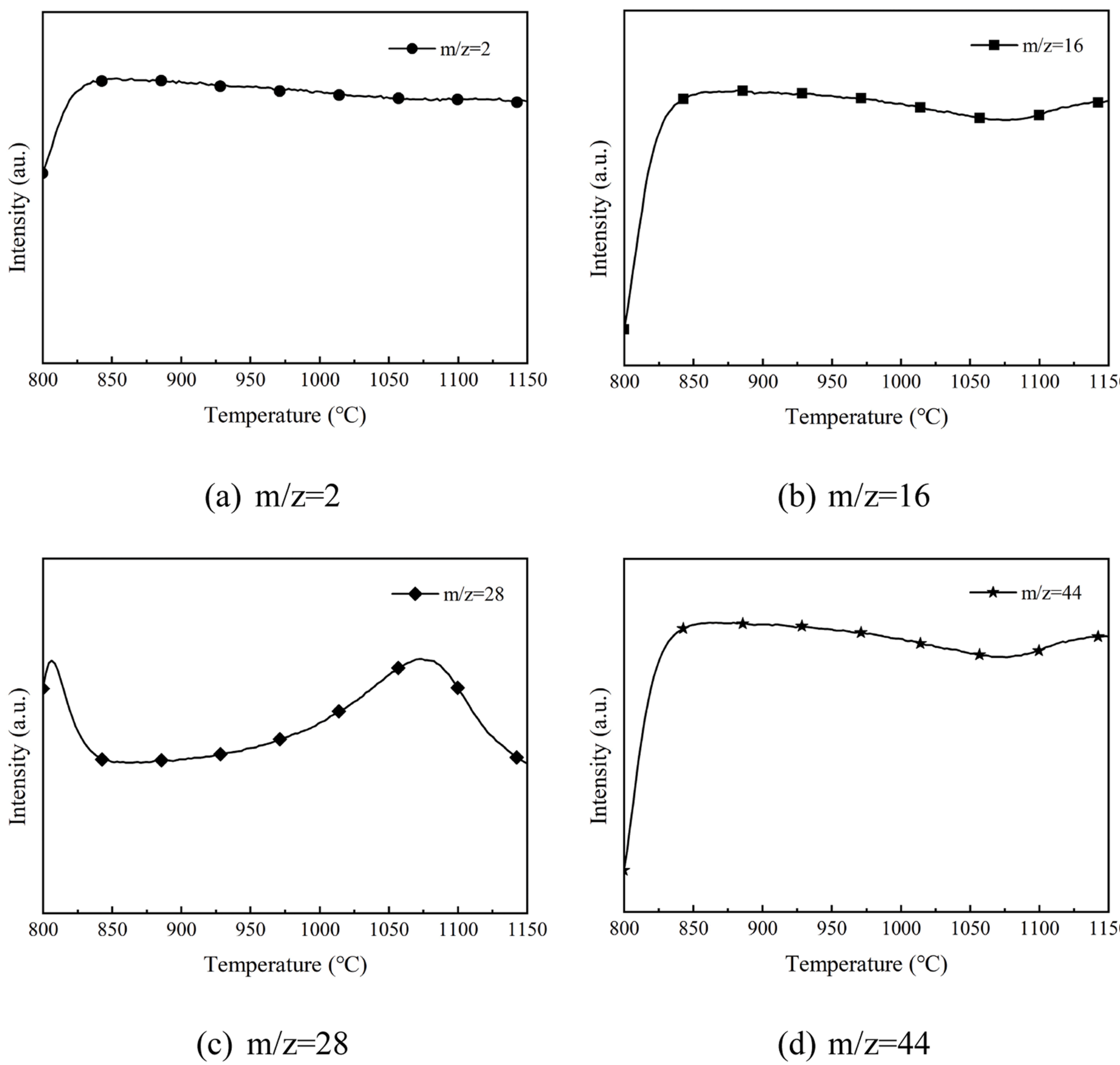

Fig. 4. TG-MS spectra of coal coke in 80 %CO_2+20 %N_2.

3.3. TG-FTIR analysis

Thermogravimetric-Fourier Transform Infrared Spectroscopy (TG-FTIR) is used to determine the gas volatilization of coal coke during gasification by measuring specific functional groups in the volatile gases, and the results are shown in Fig. 3. Since the vibration peaks of CO_2 within the gasifier appear at 4000~3400 cm^{-1}, 2500~2000 cm^{-1} and 1000~800 cm^{-1}, the vibration of which would affect the TG-FTIR results of coal coke. Thereby, the vibration changes of functional groups in the ranges of 3400~2500 cm^{-1} and 2000~1000 cm^{-1} are discussed. Table 2 shows the possible volatile gases and group types during coal coke [38–41]. The main gasification products of coal coke at different CO_2 concentrations are CO_2, CH_4, CO, alcohols, phenols and carboxylic acids, etc. In 20 %CO_2+80 %N_2, the quantities of volatile gases of coal coke are lower and the types of functional groups are fewer. Additionally, with the increase of temperature, the FTIR curves are very close to each other, which means the types and quantities of volatile gases do not change much. Moreover, the wave peak near 1330 cm^{-1} begins to become stronger at 1200 °C. With the increase of CO_2 concentration, the quantities and types of volatile gases in the coal coke gasification process become more and more abundant. It is worth noting that when the CO_2 concentration doping ratio reaches 40 %, the change of the wave peak of volatile gases near 1330 cm^{-1} is more obvious. It shows that the test signal is enhanced with increasing temperature, the half-peak width becomes larger, and the wave peaks begin to shift to higher bands. In 40 %CO_2+60 %N_2, the strongest signal near 1338 cm^{-1} occurs at 1145 °C. The strongest signal near 1338 cm^{-1} occurs at 1100 °C in 60 %CO_2+40 %N_2 and 80 %CO_2+20 %N_2. It suggests that the increase of CO_2 concentration promotes the generation of more C—O-O- functional groups on coal coke during the gasification process. At present, the mechanism of generating CO_2 complexes in coal coke during gasification is widely accepted [42]. Firstly, CO_2 is adsorbed on the surface of coal coke during gasification to form CO_2 complexes, then released from the coal coke to produce CO. In 80 %CO_2+20 %N_2, the trend of C—O-O- functional groups with temperature (Fig. 3(d)) is consistent with the strength of coal coke gasification reaction in this atmosphere (Fig. 2(d)), which suggests that the C—O-O- functional groups may be the CO-generation precursor. Xu et al. [28] used the first-principal calculations to investigate the reaction process of carbon with pure H_2O and pure CO_2 on a benzene ring, and the results pointed out that $C = O$ is the precursor for CO generation, where the dissociation process of $C = O$ from the aromatic group is the key step in the coal coke gasification process. It needs to be noted that the vibrations of C—O-O- and aromatic C—C can still be detected in the TG-FTIR test. The reason is that the aromaticity of the coal coke macromolecules is destroyed during the gasification process due to the temperature and the pre-adsorption of CO_2, and the coal coke molecules suffer structural distortions and aromatic transformations, and the breakage of the aromatic C—C results in the C—O-O- functional groups in the products escaping with gases before they are fully converted to CO [43]. Moreover, the structural distortions and aromatic ring cleavage of the coal coke molecules expose more and more active sites, which promote the pre-adsorption of CO_2 molecules, the reaction between CO_2 and coal coke, and the production of more CO. And it may be the reason for the faster decrease of the TG curve of coal coke due to the increase of CO_2 concentration.

The effects of different gasification heating rates on the TG-FTIR curves of coal coke in 80 %CO_2+20 %N_2 are shown in Fig. 3(d)–(f). With the gasification heating rate rises, the TG-FTIR wave peaks of coal coke are fewer and the peak area is lower. It is obvious that the volatilization signals of CH_4, alcohols, phenols, carboxylic acids, etc. response lately. And vibration peaks at 1348 cm^{-1} become stronger with the increase of temperature. It further indicates that the CO_2 and coal coke do not react completely during the rapid gasification process, resulting in a low gasification conversion ratio of coal coke. Therefore, an appropriate gasification heating rate is beneficial to the full reaction between CO_2 and coal coke to generate CO.

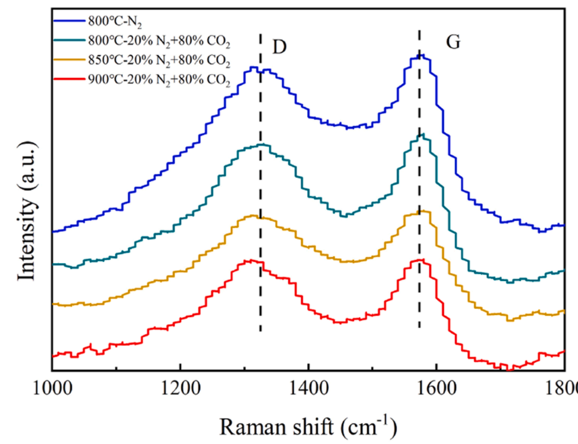

Fig. 5. *In-situ* Raman spectra of coal coke in 80 %CO_2+20 %N_2.

3.4. TG-MS analysis

The results of thermogravimetric-mass spectrometry (TG-MS) of coal coke at 800~1150 °C in 80 %CO_2+20 %N_2 are shown in Fig. 4. It can be found that the products of coal coke gasification are CO, H_2, CH_4, etc. Among them, the H_2 signal become weakened after reaching the peak at 850 °C. The H atoms in the syngas come from the residual volatile components on the surface of the coal coke and the H atoms on the edge of the coal coke molecules, which are not replenished during the gasification process, resulting in a decreasing trend in the H_2 yield. The results of $m/z = 28$ and $m/z = 44$ show the opposite trend. The signal of CO becomes stronger and then weaker with the increase of temperature. This indicates CO is main products, which formed by CO_2 and coal coke. Whereas CH_4($m/z = 16$) shows the opposite trend, first weakening and then strengthening. The reasons are that the decrease of H atoms during gasification and the activation energy of coal coke molecules reacting with CO_2 to form CO is lower compared with that of CH_4, so the signal of CH_4 shows a decreasing trend in the main stage of gasification. The signal of CO_2 also affects $m/z = 16$, so the signal at $m/z = 16$ becomes stronger again after the reaction. In summary, the main gasification product of coal coke under this gasification atmosphere is CO.

3.5. In-situ Raman analysis

The *in-situ* Raman results of coal coke under 80 %CO_2+20 %N_2 atmosphere are shown in Fig. 5. Before gasification, the G-band peak signals on the surface of coal coke are stronger, which indicates that the molecules of coal coke are still dominated by stereotyped carbon. In 80 %CO_2+20 %N_2, with the increase of temperature, the peaks of D and G bands on the surface of coal coke start to weaken and begin to approach, but the half-peak width of the D band decreases significantly. This indicates that the fixed and indeterminate carbon on the surface of coal coke begin decompose, and the decomposition rate of indeterminate carbon is faster than that of fixed carbon during coal coke gasification. This result is corroborated with the TG-FTIR results.

3.6. DFT calculations

As shown in Fig. 6 (a), based on the structural characterization of coal coke (Fig. 1), $C_{34}H_{30}O_5$ is chosen to simulate the structure of coal coke for DFT calculations, which is denoted as Model 1 [44]. As shown in Fig. 6 (b), excluding O—H vibration caused by adsorbed water molecules in the air, the IR curves of Model 1 are in high agreement with those of the FTIR curves of coal coke (Fig. 1 (a)). The electrostatic potential distributions of Model 1 and CO_2 are shown in Fig. 6 (c), (d), and the red area around the C atom in the CO_2 molecule is obvious, which indicates that the C atom carries a positive electric potential. Comparing

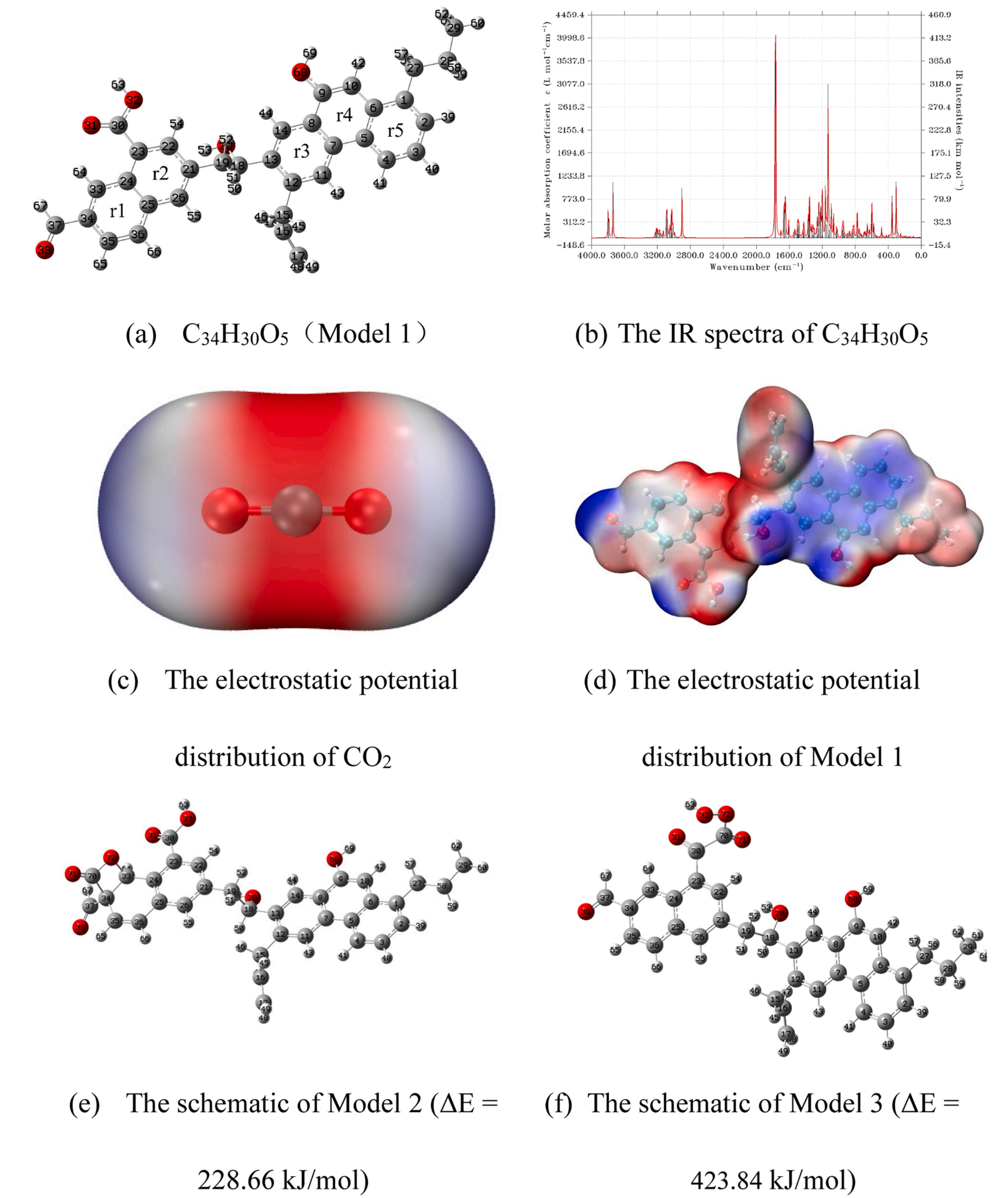

Fig. 6. Schematic diagram of molecular structure and electrostatic potential distribution.

with Model 1 (Fig. 6 (d)), blue area is obvious around the carbonyl, carboxyl, phenolic hydroxyl, and hydroxyl groups, which indicates that the potential near these group are negative and can be used as an active site for CO_2 pre-adsorption. Optimizing the model of CO_2 pre-adsorption at different adsorption sites, it is found that the structure of CO_2 pre-adsorption near the carbonyl and carboxyl groups converge, which denoted as Model 2 and Model 3, respectively. The structure and activation energy of the model after CO_2 pre-adsorption are shown in Fig. 6

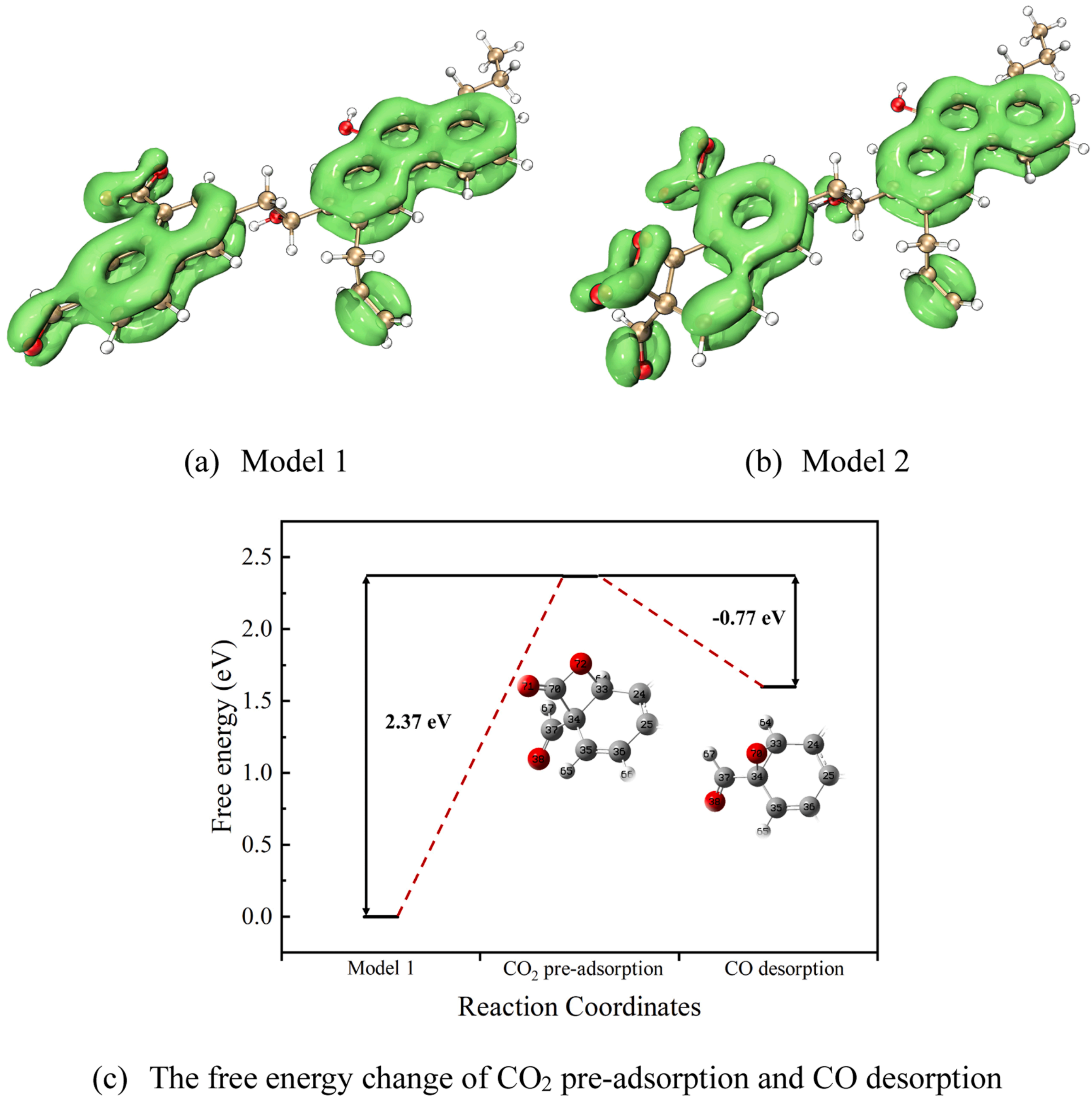

Fig. 7. The LOL results of Model 1and Model 2 (iso=0.30) and free energy change.

(e), the activation energies of the reaction are all positive, and all of them are more than 200 kJ/mol, which indicates that CO_2 adsorption on the surface of coal coke belongs to the strong adsorption reaction. The activation energy of Model 2 is lower, 228.66 kJ/mol, which indicates that CO_2 tends to be adsorbed near the carbonyl group. As shown in Fig. 6, CO_2 is not directly adsorbed on the carbonyl surface, but C70 and C34, O72 and C33 are connected to form -C-O—O-C- group without C—C bond breaking behavior. In Model 3, the C—C between O32 and C30 is broken, and then O32 and CO_2 molecules are connected to form a new -C-O—O-O- group, which may be the reason for the higher activation energy of the Model 3 reaction.

Table 3
The typical atomic mayer bond of Model 1 and Model 2.

	C24—C33	C33-C34	C34-C35	C34-C37
Model 1	1.32	1.45	1.22	0.92
Model 2	0.72	0.85	0.94	0.84

The pi electronic features of the model can be examined by the localization of the dominoed orbital localization function (LOL) calculations, which can be investigated the aromaticity of the model. The LOL analysis results of Model 1 and Model 2 are shown in Fig. 7, and the green area is the graphical representation of the pi bond (iso=0.30). As shown in Fig. 7 (a), in Model 1, the LOL-pi in the r1 ring is connected, and the connection at C22-C23 in r2 is broken, which indicates that the pi electron strength in the r1 ring is significantly stronger than in the r2 ring, so the aromaticity of r1 ring is also stronger than in the r2 ring. As shown in Fig. 7 (b), after CO_2 pre-adsorption, the LOL-pi breaks at C33 and C24 and C35 and C36, and promotes C22-C23 re-conjugation in r2 ring. This indicates that the aromaticity within the r1 ring is destroyed and the conjugation of r1 ring is significantly less than that of the r2 ring after the CO_2 pre-adsorption. It is also supported by the results of the *in-situ* Raman analysis (Fig. 5). In addition, the number of interatomic shared electron pairs can be quantitatively described by calculating the mayer bond of the atoms in the Model 1 and Model 2, and the results are shown in Table 3. The mayer bond between C24-C33, C33-C34, C34-C35, and C34-C37 in Model 1 are 1.32, 1.45, 1.22, and 0.92, respectively. In contrast, the corresponding interatomic mayer bond within Model 2 are lower, and the number of interatomic shared electron pairs becomes less. This suggests that CO_2 pre-adsorption makes the C—C bond strength within the r1 ring lower and destroys the aromaticity of the coal coke structure. Meanwhile, it has been pointed out that the CO desorption energy barrier is linearly and positively correlated with the aromaticity of the precursor [30]. As shown in Fig. 7(c), CO_2 pre-adsorption on the coal coke surface is an adsorption reaction with a free energy of 2.37 eV, while the CO desorption process is an exothermic reaction with a free energy of −0.77 eV. The entire gasification process is the endothermic reaction with 1.60 eV. Consequently, increasing temperature, the pre-adsorption of CO_2 on the coal coke surface is promoted to form C—O-O-groups, and this process would destroy the conjugation of the coal coke structure and reduce its aromaticity, which would result in structural distortion of the coal coke and aromatic C—C bond breaks at high temperatures, exposing more new reactive sites, accelerating the reaction between CO_2 and coal coke, and promoting CO desorption.

4. Conclusions

(1) The COO-group is the CO precursor from the coal coke CO_2 gasification.
(2) During the pre-adsorption of CO_2 on the surface of coal coke, C—O-O-complexes are formed, which reduce the degree of electronic conjugation of the aromatic ring pi, and the strength of the intermolecular mayer bond level is reduced. These are the reasons of destroying the aromaticity of the surface of the coal coke molecule, exposing more active sites, speeding up the gasification reaction of coal coke, and facilitating the desorption of CO.
(3) The entire gasification process is the endothermic reaction with 1.60 eV.

CRediT authorship contribution statement

Hui Luo: Writing – original draft, Validation, Software, Methodology, Investigation. **Yaqiong Wang:** Investigation. **Weiwei Xuan:** Writing – review & editing, Software, Funding acquisition. **Jiansheng Zhang:** Writing – review & editing, Methodology, Investigation, Funding acquisition.

Declaration of competing interest

The authors declare that they have no known competing financial interests or personal relationships that could have appeared to influence the work reported in this paper.

Acknowledgements

This work was financially supported by the Science and Technology Major Special Program of Shanxi Province [Grant No. 202201090301002] and the Young Scholars Development Program of Shanxi Research Institute of Huairou Laboratory [Grant No. 2023SY3003].

Data availability

Data will be made available on request.

References

[1] Q. Li, Q. Wang, J. Hou, J. Zhang, Y. Zhang, Aggregating structure in coal water slurry studied by eDLVO theory and fractal dimension, Front. Energy 17 (2) (2023) 306–316.
[2] Q. Li, Y. Wang, J. Xie, L. Liang, W. Zhang, Dewatering promoting of carbon-rich coal gasification coarse slag by size reduction with surface modification, Int. J. Coal Prep. Util. (2024).
[3] Z.H. Chen, D.G. Lai, L.Q. Bai, Y. Tian, S.Q. Gao, G.W. Xu, et al., Methane-rich syngas production in an integrated fluidized bed by coupling pyrolysis and gasification of low-rank coal, Fuel Process. Technol. 140 (2015) 88–95.
[4] V.S. Naidu, P. Aghalayam, S. Jayanti, Evaluation of CO_2 gasification kinetics for low-rank Indian coals and biomass fuels, J. Therm. Anal. Calorim. 123 (1) (2016) 467–478.
[5] K. Jayaraman, I. Gokalp, Gasification characteristics of petcoke and coal blended petcoke using thermogravimetry and mass spectrometry analysis, Appl. Therm. Eng. 80 (2015) 10–19.
[6] C. Xu, S. Hu, J. Xiang, L. Zhang, L. Sun, C. Shuai, et al., Interaction and kinetic analysis for coal and biomass co-gasification by TG-FTIR, Bioresour. Technol. 154 (2014) 313–321.
[7] K.B. Kabir, A. Tahmasebi, S. Bhattacharya, J. Yu, Intrinsic kinetics of CO_2 gasification of a Victorian coal char, J. Therm. Anal. Calorim. 123 (2) (2016) 1685–1694.
[8] Q. Yao, M. Ma, Y. Liu, L. He, M. Sun, X. Ma, Pyrolysis characteristics of metal ion-exchanged Shendong coal and its char gasification performance, J. Anal. Appl. Pyrolysis (2021) 155.
[9] H.C. Ong, W.H. Chen, Y. Singh, Y.Y. Gan, C.Y. Chen, P.L. Show, A state-of-the-art review on thermochemical conversion of biomass for biofuel production: a TG-FTIR approach, Energy Convers. Manag. 209 (2020).
[10] Z. Zhang, B. Yi, Z. Sun, Q. Zhang, H. Feng, H. Hu, et al., Reaction process and characteristics for coal char gasification under changed CO_2/H_2O atmosphere in various reaction stages, Energy (2021) 229.
[11] C. Lan, Q. Lyu, X. Liu, M. Jiang, Y. Qie, S. Zhang, Thermodynamic and kinetic behaviors of coke gasification in N_2-CO-CO_2-H_2-H_2O, Int. J. Hydrog. Energy 43 (42) (2018) 19405–19413.
[12] D.G. Roberts, D.J. Harris, Char gasification in mixtures of CO_2 and H_2O: competition and inhibition, Fuel 86 (17–18) (2007) 2672–2678.
[13] Z. Yang, M. Gao, Y. Bai, F. Li, Model establishment for the kinetic evaluation of synergistic effect on the coal char gasification with H_2O and CO_2 mixtures, Appl. Therm. Eng. 118 (2017) 682–690.
[14] K. Jayaraman, I. Gokalp, S. Jeyakumar, Estimation of synergetic effects of CO_2 in high ash coal-char steam gasification, Appl. Therm. Eng. 110 (2017) 991–998.
[15] W. Xuan, D. Xia, *In situ* minerals transformation study of low-temperature ash, Energy Fuels 32 (1) (2018) 336–341.
[16] Q. Song, H. Zhao, J. Jia, L. Yang, W. Lv, Q. Gu, et al., Effects of demineralization on the surface morphology, microcrystalline and thermal transformation characteristics of coal, J. Anal. Appl. Pyrolysis (2020) 145.
[17] P. Zong, Y. Jiang, Y. Tian, J. Li, M. Yuan, Y. Ji, et al., Pyrolysis behavior and product distributions of biomass six group components: starch, cellulose, hemicellulose, lignin, protein and oil, Energy Convers. Manag. (2020) 216.
[18] F. Chen, B. Yan, N. Liu, J. Zhang, J. Zhu, H. Zhang, et al., Bimetallic oriented catalytic fast pyrolysis of lignin research based on PY-GC/MS, Biomass Convers. Biorefin. 10 (4) (2020) 1315–1325.
[19] W.H. Chen, C.W. Wang, H.C. Ong, P.L. Show, T.H. Hsieh, Torrefaction, pyrolysis and two-stage thermodegradation of hemicellulose, cellulose and lignin, Fuel (2019) 258.
[20] S. Wang, S. Zhao, X. Cheng, L. Qian, B. Barati, X. Gong, et al., Study on two-step hydrothermal liquefaction of macroalgae for improving bio-oil, Bioresour. Technol. (2021) 319.
[21] J. Cheng, Y. Zhang, T. Wang, P. Norris, W.Y. Chen, W.P. Pan, Thermogravimetric-fourier transform infrared spectroscopy-gas chromatography/mass spectrometry study of volatile organic compounds from coal pyrolysis, Energy Fuels 31 (7) (2017) 7042–7051.
[22] Z. Lei, Z. Cheng, Q. Ling, X. Liu, P. Cui, Z. Zhao, Investigating the trigger mechanism of Shenfu bituminous coal pyrolysis, Fuel (2022) 313.
[23] T. Su, Y. Song, X. Lan, Product characteristics and interaction mechanism in low-rank coal and coking coal co-pyrolysis process, J. Chem. Eng. Jpn. 53 (4) (2020) 167–176.
[24] H. Zhu, G. Yu, Q. Guo, X. Wang, *In situ* Raman spectroscopy study on catalytic pyrolysis of a bituminous coal, Energy Fuels 31 (6) (2017) 5817–5827.
[25] S. Yan, D. Xia, W. Xuan, New insight into enhancement effect of supercritical water on scrap tire depolymerization: a study based on ReaxFF-MD simulation and DFT method, Fuel Process. Technol. (2020) 200.
[26] G.Y. Li, F. Wang, J.P. Wang, Y.Y. Li, A.Q. Li, Y.H. Liang, ReaxFF and DFT study on the sulfur transformation mechanism during the oxidation process of lignite, Fuel 181 (2016) 238–247.
[27] W. Xuan, J. Gao, Z. Ma, C. Cao, S. Yan, Q. Wang, Synergistic mechanism and radicals interaction of the co-pyrolysis of lignite and PE based on ReaxFF-MD and DFT, Energy (2024) 289.
[28] R. Xu, B. Dai, W. Wang, J. Schenk, A. Bhattacharyya, Z. Xue, Gasification reactivity and structure evolution of metallurgical coke under H_2O/CO_2 atmosphere, Energy Fuels 32 (2) (2018) 1188–1195.
[29] M. Dong, L. Feng, B. Qin, Characteristics of coal gasification with CO_2 after microwave irradiation based on TGA, FTIR and DFT theory, Energy (2023) 267.
[30] D. Zhao, H. Liu, P. Lu, H. Yu, M. Qin, A DFT study of the mechanism of H transfer during steam gasification, Combust. Flame 219 (2020) 327–338.

[31] L. Zhang, T. Wang, M. Zhang, Q. Liu, Y. She, S. Wu, et al., Synergistic degradation of Tris (2-Chloroethyl) Phosphate (TCEP) by US/Fenton system: experimental, DFT calculation and toxicity evaluation, Environ. Sci. Pollut. Res. Int. 31 (27) (2024) 39120–39137.
[32] H. Luo, S. Zhao, A. Ma, K. Sun, Y. Zhu, Z. Sun, Influence of flue gas components on the mercury adsorption/oxidation by mechanochemical S_2Cl_2-modified sawdust coke, Fuel 336 (2023).
[33] X. Zou, M. Zhai, D. Yang, G. Liu, T. Wang, L. Guo, et al., New insights into the mechanism of biomass char steam gasification process by oxygen-containing functional group as aromatic carbon boundaries: experimental and DFT study, Chem. Eng. J. (2023) 465.
[34] J. Lv, Y. Wang, Y. Bao, Y. Yang, O. Kawa, X. Lin, et al., Understanding the slag transformation behaviors during entrained-flow gasification based on comparative analysis of slag properties, Asia-Pac. J. Chem. Eng. 17 (1) (2022).
[35] J. Cai, W. Zheng, M. Luo, C. Kuang, Evaluation of the CO_2 gasification of residual char under a regeneration atmosphere via calcium-based chemical looping gasification, Chem. Eng. Process. Process Intensif. (2021) 168.
[36] P.I. Kyesmen, W. Pooe, N. Nombona, M. Diale, Effects of heating rate and deposition cycle on the structural, optical, and photoelectrocatalytic properties of electrodeposited hematite films, Mater. Today Commun. 40 (2024).
[37] Y.X. Yu, J. Kong, M.J. Wang, L.P. Chang, Structure and oxidation reactivity of char: effects of pyrolysis heating rate and pressure, J. Fuel Chem. Technol. 46 (9) (2018) 1025–1035.
[38] Y. Wang, Z. Ge, F. Shang, C. Zhou, S. Guo, C. Ren, Kinetic analysis of CO_2 gasification of corn straw, Renew. Energy 203 (2023) 219–227.
[39] X. Fu, J. Li, B. Yan, G. Chen, Hou La, J. Tao, Insights into biomass mild gasification based on mass-energy balance: establishing condition, thermodynamic mechanisms, and product properties, Chem. Eng. J. (2024) 481.
[40] J. Chen, X. Pan, H. Li, H. Jin, J. Fan, Molecular dynamics investigation on the gasification of a coal particle in supercritical water, Int. J. Hydrog. Energy 45 (7) (2020) 4254–4267.
[41] B. Lin, Y. Wang, Inconsistency of economic growth and electricity consumption in China: a panel VAR approach, J. Clean. Prod. 229 (2019) 144–156.
[42] Z. Liu, Y. Li, Insight into competing reaction mechanism of char oxidation by DFT study, J. Phys. Chem. C. 238 (2022).
[43] Q. Luo, Y. Bai, J. Wei, X. Song, P. Lv, J. Wang, et al., Insights into the oxygen-containing groups transformation during coal char gasification in H_2O/CO_2 atmosphere by using ReaxFF reactive force field, J. Energy Inst. 109 (2023).
[44] Y. Zhang, P. Shu, J. Deng, Z. Duan, L. Li, L. Zhang, Analysis of oxidation pathways for characteristic groups in coal spontaneous combustion, Energy (2022) 254.